CHIN. PHYS. LETT. Vol. 34, No. 3 (2017) 034211

Interference from Two-Photon Sources in Silica-on-Silicon Circuits at Telecom Wavelength *

Xing-Yun Li(黎星云), Lu Qin(秦璐), Jia-Shun Zhang(张家顺), Mei-Zhen Ren(任梅珍), Jun-Ming An(安俊明), Xiao-Hong Yang(杨晓红), Xing-Sheng Xu(许兴胜)**

State Key Laboratory of Integrated Optoelectronics, Institute of Semiconductors, Chinese Academy of Sciences, Beijing 100083

(Received 27 October 2016)

The integrated photonic chip is a promising way to realize future quantum technology. Here we demonstrate a two-photon interference in the standard telecommunication band on a silica-on-silicon integrated photonic chip. Two identical photons in the 1.55 μm band, which are indistinguishable in spatial, frequency and polarization, are generated by type-I collinear spontaneous parametric down-conversion via bismuth borate. The silica-on-silicon integrated chip, which has an insertion loss less than 1 dB, is a Mach–Zehnder interferometer with a thermo-optic phase shifter. A high visibility of 100% in the classical interference and 99.2% in the two-photon interference is achieved, indicating that the two-photon interference with high interference visibility on the chip is attained successfully.

PACS: 42.50.St, 42.65.Lm, 42.79.Gn DOI: 10.1088/0256-307X/34/3/034211

Compared with classical theory, quantum information technology possesses its great potential for performing certain tasks in quantum information security,[1] computation,[2] and measurement.[3] Photon quantum technologies require single photon sources, single photon detectors and sophisticated optical circuits with high-visibility classical and quantum interference.[4–6] Quantum photonic circuits[7,8] have been fabricated using silicon-based waveguide materials, such as silica-on-silicon[9,10] and silicon-on-insulator (SOI),[11,12] where the directional coupler (DC)[13,14] or the multi-mode interference (MMI)[12,15] is the key component in the integrated quantum photonic chip. For example, miniaturized integrated quantum circuits were realized to actualize the first integrated optical control-NOT gate, achieving a high fidelity close to the theoretical value.[9] After that, a near-unit fidelity quantum interference and a two-photon entangling logic operation were also reported with a similar silica-on-silicon chip.[16] Hong-Ou-Mandel interference dip was obtained in the UV laser written optical circuits fabricated in a suitable stack of doped silica layers on a silicon substrate.[17] Such experiments demonstrating phase control in integrated, path-encoded waveguide systems and photons' quantum circuits were mainly operated at wavelengths around 800 nm on silica-on-silicon chips. However, it is quite an important issue to develop the two-photon interference technique in the standard telecom wavelength, which is exactly more suitable for future application.[18–20] However, in the aspects of integrated optical circuit, quantum interference and manipulation of entanglement in the 1.55 μm band has been conducted in an SOI chip. A raw visibility of only $V = 81.8 \pm 1.3\%$ for two-photon fringes could be obtained by using a Mach–Zehnder interferometer (MZI) in an SOI chip in the 1.55 μm band for its coupling loss as well as propagation loss.[12] As a matter of fact, silica-on-silicon chips often possess advantages of less insertion loss and better fiber coupling, while there are still few reports on photon interference in 1.55 μm region based on silica-on-silicon waveguides to date. Here we demonstrate the manipulation of an entangled state utilizing the silica-on-silicon system in 1.55 μm, and a high visibility two-photon interference[21] of 99.2% which is higher than previous implementations.

As shown in Fig. 1(a), our silica-on-silicon integrated photonic chip is an MZI, which comprises two directional couplers and a thermo-optic phase shifter modified on-chip quantum state. MZI devices have been well studied for classical operation, while their capability for quantum operation will be studied here, where interference occurs between photons as well as self-interference. The silica-on-silicon integrated quantum photonic chip was fabricated by standard semiconductor techniques for planar lightwave circuit (PLC).[22] Firstly, a 15 μm layer of thermally grown undoped silica was deposited on a silicon substrate as a buffer. Then a 6 μm waveguide layer of silica doped with germanium was deposited on the buffer by plasma-enhanced chemical vapor deposition (PECVD). After the waveguide was fabricated with PLC techniques, a 15 μm cladding layer of boron phosphorous silicate glass (BPSG) with a refractive index matching to that of the buffer was overgrown on the core layer. BPSG was used as a cladding layer for its superior liquidity as well as flatness in comparison with silica. The schematic geometry of two silica-on-silicon waveguides of the MZI device is shown in Fig. 1(b). Finally, a pair of Ti/Au electrodes was fabricated as a thermo-optic phase shifter. It was possible to tune the internal phase delay of the MZI device by varying the voltage across the phase shifter. In our experiment, four ports of the MZI device were formed by scribing and coupled respectively to two single-mode fiber arrays with 127 μm

*Supported by the National Natural Science Foundation of China under Grant Nos 61627820, 61575191 and 61275045, and the National Basic Research Program of China under Grant Nos 2016YFA0301200, 2013CB632105.

**Corresponding author. Email: xsxu@semi.ac.cn

© 2017 Chinese Physical Society and IOP Publishing Ltd

spacing, which was placed in a V-type optical fiber positioning groove. The waveguide ports and fiber array were stuck by ultraviolet curing adhesive. In order to achieve a single mode operation at 1550 nm in the 6 μm × 6 μm waveguide, the refractive index contrast (Δ) between waveguide core and cladding was set to be 0.75%, which could be extracted from the formula $\Delta = (n_{\text{core}}^2 - n_{\text{cladding}}^2)/(2n_{\text{core}}^2)$, where n_{core} and n_{cladding} represent the refractive indexes of the waveguide layer and the cladding layer, respectively. The optimized DC was designed to be two 6-μm-wide waveguides with a 2.8-μm gap. Extensive simulations using beam propagation method (BPM)[23] were performed, the simulated transverse mode-field profile in such a silica waveguide structure is displayed in Fig. 1(c), and the optical field propagation simulation in the DC with a coupling ratio of 50:50 is shown in Fig. 1(d).

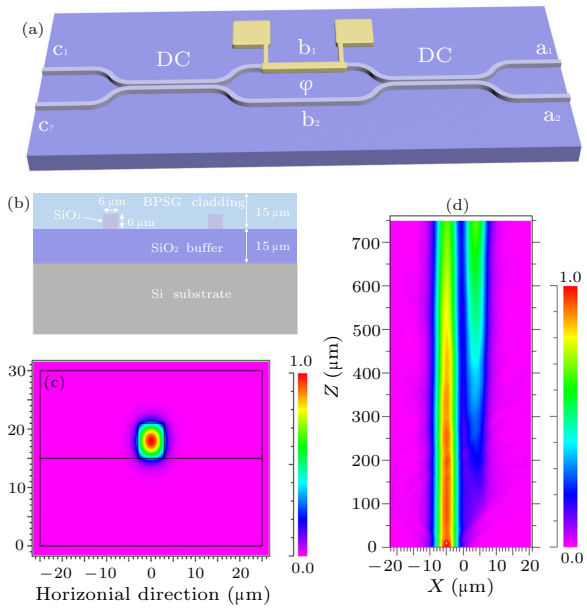

Fig. 1. Silica-on-silicon integrated MZI chip. (a) A schematic diagram of the MZI device, consisting of two directional couplers and a voltage controlled thermo-optic phase shifter. (b) A schematic cross-section of the MZI device. (c) Simulated transverse mode profile on the designed single mode silica waveguide structure. (d) Optical field distribution of the DC design with 6-μm waveguide width and 2.8-μm gap by BPM simulation at 1550 nm.

Pairs of indistinguishable single photons at a wavelength of 1550 nm were produced in a type-I spontaneous parametric down-conversion (SPDC)[24–26] using a 3-mm-thick bismuth borate BiB_3O_6 (BiBO) crystal.[27–29] Compared with barium boron oxide (BBO), BiBO possesses its own advantages such as stable physical properties, high optical damage threshold, and large nonlinear optical coefficient at 1550 nm telecom optics. Setup of the experiment is illustrated in Fig. 2, where a 1550 nm photon pair was generated non-deterministically from the crystal pumped by a ∼140 fs, 80 MHz repetition rate 775 nm Ti:Sapphire laser. For the purpose of satisfying the type-I collinear phase matching of the BiBO crystal, the polarization and direction of the pump laser were adjusted carefully by rotating the half wave plate and the BiBO crystal. Then two indistinguishable photons at 1550 nm wavelength, which shared the same properties in three degrees of freedom: spatial, frequency and polarization, were generated by SPDC in the BiBO crystal. After that, the photon pairs were filtered by a 12-nm-wide bandpass interference filter and collected by a fiber-optic collimator with aspheric lens (f = 11 mm). To ensure the optimum collection, we adjusted the collimator carefully to maintain alignment with the down-converted photons. Then the photon-pairs were fed into a single-mode fiber (SMF), which was coupled to the input port of the MZI device. Once photons traversed the MZI device, they would be collected by an SMF array and sent to two single-photon detectors (SPDs). Photons were finally detected by two SPDs of InGaAs avalanche photo-diode (single-photon counting modules (SPCMs)) at near-infrared wavelengths and were analyzed by a time-correlated single photon counting (TCSPC) system. Quantum efficiency of the SPDs could reach 30% at the repetition frequency of 50 MHz. Coincidence detection between two output ports of the chip could be performed in TCSPC (TimeHarp 260) with 25 ps base resolution.

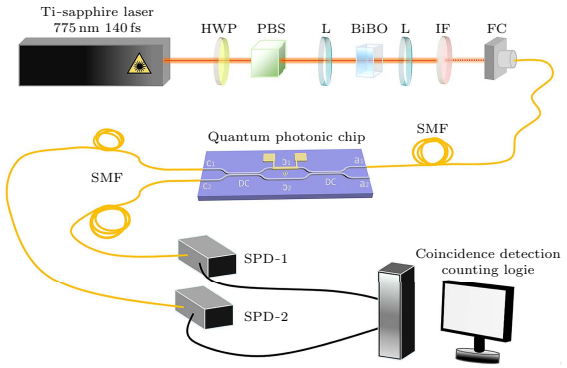

Fig. 2. Schematic diagram of the experimental setup to characterize the MZI chip. HWP: half wave plate; PBS: polarizing beam splitter; L: lens; BiBO: BiB_3O_6 crystal; IF: interference filter; FC: fiber-optic collimator; SMF: single-mode fiber; SPD: InGaAs single-photon detector; and TCSPC system, a time-correlated single photon counting system.

In the first instance, the fabricated MZI chip was characterized by classical light. The light source was a continuous wave (CW) laser at 1550 nm wavelength. The insertion loss of this device was measured to be less than 1 dB at 1550 nm. Classical interference was observed in the transmission of laser through the MZI device by tuning the phase of the phase shifter. Classical interference was quantified by the power of two output ports of the device as on-chip phase ϕ was varied. The power of two output ports varied sinusoidally with a periodicity of 2π, by applying a voltage from 0 V to 7 V across the thermo-optic phase shifter, where the on-chip phase was in proportion to the square of applied voltage. The classical interference fringes are displayed in Fig. 3(a), where the measurement data points were fitted to two sine curves. The periods of the two curves were, respectively, 36.7 V^2 for port c_1 and 36.0 V^2 for port c_2. The visibilities of the classical interference curves were 100±0.8% for output port c_1 and 100±0.9% for port c_2. The visibility was computed by $V = (N_{\max} - N_{\min})/N_{\max}$, where the max-

imum value $N_{\max}$ and the minimum value $N_{\min}$ were extracted from the fitting sine curves, respectively.

In the second instance, we characterized the MZI photonic chip by using SPDC quantum light source. Since 1550 nm photon pairs have been generated in BiBO crystal by SPDC, correlation of the photon pairs could be demonstrated by coincidence detection in a beam splitter. We first used a 1550 nm 50:50 beam splitter to replace quantum photonic chip in the experimental setup. Photon pairs were injected into one port of the beam splitter, and coincidence detection was performed by TCSPC. Output of the SPD1 was employed as the trigger to start the timer in TCSPC and to record the output of SPD2 in a relative delay time. After a time period of 12.5 ns (determined by the repetition frequency of the pumping laser of Ti:sapphire), the recorder start–stop events were classified at distinct time, and the time bin was set 25 ps in this experiment. At relative zero delay time, there was a coincident peak. At delay periodic time of 12.5 ns relative to the coincident peak, the recorded counts were accidental coincidence. It was found that the coincidence peak at relative zero delay time was higher than accidental coincidence peaks, which indicated the correlation of the down-converted photon pairs.

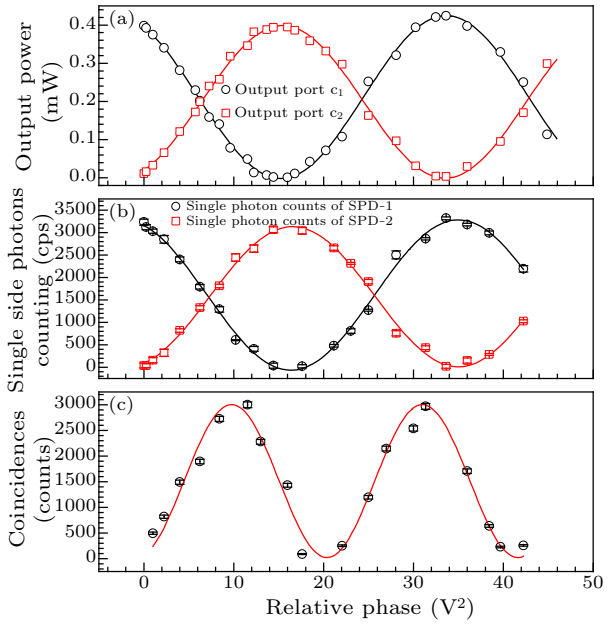

Fig. 3. Classical and two-photon interference measurements, varying the on-chip phase ϕ. (a) Transmission of the continuous wave laser shows the classical interference, where the black line represents the output power of port c_1 and the red line represents that of port c_2. The x-axis represents the varied phase by the applied voltage across the thermo-optic phase shifter, where the on-chip phase was in direct proportion to the square of applied voltage, and the y-axis represents the output power of two output ports c_1 and c_2. (b) Single side photon count rates collected from SPD1 (black line) and SPD2 (red line) as a function of the phase changing both show interference fringes. The y-axis represents single side photons counting at unit time (1 s). (c) Two-photon coincidence count rates as a function of the varied internal phase by applying different voltages show two-photon interference fringe. The y-axis represents two-photon coincidence counts obtained from counting logic. Error bars are given by the Poissonian statistics, based on the raw coincidences.

Then, down-converted photon pairs were injected into the input port a of the fabricated MZI chip. In the experiment, as the internal phase of the MZI device was changed, the single side counting was recorded in two InGaAs SPDs, which were, respectively, connected to the output ports c_1 and c_2. When the voltage was 0 V, single photon counting rate was 3233 counts per second (cps) (maximum value) for port c_1 recorded in SPD1, and 38 cps (minimum value) for port c_2 recorded in SPD2, where background counting has already been subtracted from all recording values. When the voltage changed to 3.8 V, the single photons' counting rates for two ports converted, in which 35 cps was recorded in SPD1, and 3063 cps was recorded in SPD2. These recording values are displayed in Fig. 3(b), and fitted with $C_{c_1c_2} \propto (1 \pm \cos\phi)$, respectively. One period of the interference fringes c_1 was 37.2 V^2 for port c_1 and 36.8 V^2 for port c_2, respectively, just similar to the classical interference. In the meantime, net visibilities of 100±1.2% for output port c_1 and 99.7±1.2% for port c_2 could be attained from the fitting curves.

Meanwhile, the coincidence detection was proceeding in TCSPC under different voltages. The coincidence at relative zero delay time was significantly higher than the others, which proved that the recorded photon pairs transmitted through the MZI circuit were correlated. When no voltage was applied to the thermo-optic phase shifter, outputs of the MZI device had the largest difference, resulting in the minimum of the coincidence count. When the voltage was regulated to 3.4 V, two outputs of the MZI device became comparable, attaining the maximum of the coincidence count. The coincidence count at relative zero delay time as a function of square of voltage was summed up and displayed in Fig. 3(c). The total coincidence count was extracted by summing contributions of the 13 time bins (time bin width of 25 ps) covering the coincidence peak. In Fig. 3(c), we fitted the curve with a sine function, which is in agreement with $P \propto (1 - \cos 2\phi)$. From the fitting curve, the visibility of 99.2±3.2% could be attained, where the standard error of 3.2% represented the deviation of the fitting curve from raw data. Comparing Fig. 3(c) with Figs. 3(a) and 3(b), two-photon interference fringe varied following $\cos 2\phi$ with a periodicity of 20.2 V^2, which was around half the ones in the single side interference and classical interference fringe.

The input two-photon state was $\Psi_{\text{in}} = |20\rangle$, which gave rise to two-photon interference at the first DC. After the first DC, the two-photon state was transformed to $\Psi_{\text{middle}} = [(|20\rangle - |02\rangle)/\sqrt{2} + i|11\rangle]/\sqrt{2}$, which was a partly entangled state. After passing through the phase shifter on one arm, a 2ϕ phase-shift was applied to the biphoton component. Then, the two-photon state interfered on the second DC, and the output state was $\Psi_{\text{out}} = \frac{1}{\sqrt{2}}(\frac{e^{i\phi}-1}{2})^2 \times \frac{|20\rangle}{\sqrt{2}} - \frac{1}{\sqrt{2}}(\frac{e^{i\phi}+1}{2})^2 \times \frac{|02\rangle}{\sqrt{2}} + i\sqrt{2}(\frac{e^{i\phi}-1}{2})(\frac{e^{i\phi}+1}{2})|11\rangle$, resulting interference fringes on single side photons counting and two-photon interference fringes on coincidence counting with varying MZI phase. Furthermore, this process can be explained in another way. The input state is $\frac{1}{\sqrt{2}}(\hat{a}_1^+)^2|0\rangle$, where $\hat{a}_1^+$ denotes the cre-

ation operators of the photons at the input ports a_1 of the chip. After the first directional coupler, the two-photon state is transformed to $\frac{1}{\sqrt{2}}(\widehat{b}_1^+ + i\widehat{b}_2^+)^2|0\rangle$, where $\widehat{b}_1^+$ and $\widehat{b}_2^+$ represent the creation operators of the photons at the output ports of the first DC. It is corresponding to $[(|20\rangle - |02\rangle)/\sqrt{2} + i|11\rangle]/\sqrt{2}$ mentioned above, which is a partly entangled state. The phase shifter on one arm of the MZI device provides a phase shift of ϕ on the quantum state. Then, the two photons propagate through the second DC and the quantum state at output ports c_1 and c_2 can be expressed by $\frac{1}{\sqrt{2}}\frac{1}{\sqrt{2}}[(\widehat{c}_1^+ + i\widehat{c}_2^+) + i(\widehat{c}_2^+ + i\widehat{c}_1^+)e^{i\phi}]^2|0\rangle = \frac{1}{2}[\widehat{c}_1^+(1 - e^{i\phi}) + i\widehat{c}_2^+(1 + e^{i\phi})]^2|0\rangle$, where $\widehat{c}_1^+$ and $\widehat{c}_2^+$ represent the creation operators of the photons at the output ports of the second DC. Then the single side photon counting should follow $C_{c_1c_2} \propto (1 \pm \cos\phi)$ and the probability of coincidence detections was $P \propto (1 - \cos 2\phi)$, which corresponds to the fitting curves in Fig. 3 as mentioned above. From the expression of state Ψ_{middle}, we could infer that the presence of the $|11\rangle$ state will limit the visibility of contrast ratio of the interference fringes. In consideration of phase varying in an MZI chip, when specifically setting $\phi = 0$ or $\phi = \pi$, the $|11\rangle$ component in the output state Ψ_{out} would be completely canceled, resulting in theoretical interference visibility of 100%. In our experiment, the high visibility of the classical and two-photon interference in Fig. 3 closing to the theoretical value mainly benefited from the degree of indistinguishability of the photon pairs and the quality of the interferometer. The two-photon source used in this measurement was generated by the type-I collinear SPDC, resulting in degenerated frequency and two photons fully indistinguishable. On the other hand, the fabricated silica-on-silicon MZI had low insertion loss (∼1 dB), and silica waveguide maintained single mode transmission with high stability to minimize intermodal group dispersion. Moreover, another factor played a certain influence in high visibility, where appropriate numbers of time bins were chosen to accumulation of coincidence count to decrease noise counts. These factors make high degree visibility of non-classical interference, which is critical for large-scale implementations of quantum photonic circuits. A standard error of 3.2% in Fig. 3(c) could be attained from the fitting error of parameters in the sine function. The fitting function was expressed as $y = y_0 + A\sin[\pi(x - x_c)/\omega]$, thus the visibility could be extracted from $V = (N_{\max} - N_{\min})/N_{\max} = 2A/(y_0 + A)$. Meanwhile, the standard error of $y_0(\Delta y_0)$ and $A(\Delta A)$ could be calculated by the least square method in the fitting process. Then the standard of visibility was attained from $\Delta V = \sqrt{[(\frac{\partial V}{\partial y_0})_A \times \Delta y_0]^2 + [(\frac{\partial V}{\partial A})_{y_0} \times \Delta A]^2}$. A slightly high standard error may be caused by the immature cutting quality of the BiBO crystal, leading to a phase mismatch in our system. Nevertheless, due to the low insertion loss of our device, the coincidence counts could also been attained after a long time accumulation.

In conclusion, we have realized a two-photon interference with a high visibility in the standard telecom wavelength range in a silica-on-silicon waveguide photonic circuit. The silica-on-silicon photonic circuit with an integrated MZI consists of two directional couplers and a thermo-optic phase shifter. The insertion loss is successfully reduced to 1 dB, which is beneficial to attain a high interference visibility at near-infrared wavelengths. Two identical correlated photons in the 1.55 μm band prepared by type-I spontaneous parametric down-conversion in the BiBO crystal are used to characterize the silica-on-silicon MZI. In our experiments, two-photon interference with visibility reaching up to 99.2% on silica-on-silicon chip in 1.55 μm band is realized. Large-scale integrated quantum photonic technologies will require quantum sources, waveguide circuits and single photon detector integrated on a chip. In recent years, photon pairs generated by spontaneous four-wave mixing in on-chip integrated waveguides, such as silicon microring and waveguides, have been demonstrated. Moreover, the pump laser performed by Ⅲ–Ⅴ material bonding to silicon chip would also be integrated on one chip. Such an MZI quantum circuit with high quantum-interference visibility on the silica-on-silicon system in telecom wavelength will be a key building block in fully integrated photonic quantum technologies.

References

[1] Gisin N and Thew R T 2010 *Electron. Lett.* **46** 965
[2] Thompson M et al 2011 *IET Circ. Dev. Syst.* **5** 94
[3] Hong C K, Ou Z Y and Mandel L 1987 *Phys. Rev. Lett.* **59** 2044
[4] Rosfjord K M et al 2006 *Opt. Express* **14** 527
[5] Chen J R, Zhang W, Zhou Q et al 2010 *Chin. Phys. Lett.* **27** 124208
[6] Wang P X, Zhou Q, Zhang W et al 2012 *Chin. Phys. Lett.* **29** 054215
[7] Peruzzo A, Lobino M, Matthews J C et al 2010 *Science* **329** 1500
[8] Matthews J C F, Politi A, Bonneau D et al 2011 *Phys. Rev. Lett.* **107** 163602
[9] Politi A, Cryan M J, Rarity J G et al 2008 *Science* **320** 646
[10] Carolan J, Harrold C, Sparrow C et al 2015 *Science* **349** 711
[11] Silverstone J W, Bonneau D, Ohira K et al 2013 *Nat. Photon.* **8** 104
[12] Bonneau D, Engin E, Ohira K et al 2012 *New J. Phys.* **14** 045003
[13] Zhang Y, McKnight L, Engin E et al 2011 *Appl. Phys. Lett.* **99** 161119
[14] Matthews J C F, Politi A, Stefanov A et al 2009 *Nat. Photon.* **3** 346
[15] Poulios K, Fry D, Politi A et al 2013 *Opt. Express* **21** 23401
[16] Laing A, Peruzzo A, Politi A et al 2010 *Appl. Phys. Lett.* **97** 211109
[17] Marshall G D, Politi A, Matthews J C F et al 2009 *Opt. Express* **17** 12546
[18] Li X Y, Yang L, Cui L et al 2008 *Opt. Lett.* **33** 593
[19] Yang L 2011 *Acta Phys. Sin.* **60** 2509 (in Chinese)
[20] Yang L, Ma X X, Cui L et al 2011 *Acta Phys. Sin.* **60** 308 (in Chinese)
[21] Rarity J G, Tapster P R, Jakeman E et al 1990 *Phys. Rev. Lett.* **65** 1348
[22] Yuan P, Wu Y D, Wang Y et al 2015 *J. Semicond.* **36** 084005
[23] Zhang L M, Lu D, Li Z S et al 2016 *J. Semicond.* **37** 124005
[24] Bonneau D, Lobino M, Jiang P et al 2012 *Phys. Rev. Lett.* **108** 053601
[25] Noh T G, Kim H, Youn C et al 2006 *Opt. Express* **14** 2805
[26] Cho S B and Noh T G 2007 *Opt. Express* **15** 7591
[27] Huo G, Zhang T, Wan R et al 2013 *Optik* **124** 6627
[28] Huo G, Wang Y and Zhang M 2015 *Appl. Phys.* B **120** 239
[29] Zhang M and Huo G 2014 *Opt. Eng.* **53** 086105